CARBON 50 (2012) 784–790

Available at www.sciencedirect.com

SciVerse ScienceDirect

journal homepage: www.elsevier.com/locate/carbon

Stacking dependent electronic structure and transport in bilayer graphene nanoribbons

Xiaoliang Zhong [a], *Ravindra Pandey* [a,*], *Shashi P. Karna* [b]

[a] *Department of Physics, Michigan Technological University, Houghton, MI 49931, USA*

[b] *US Army Research Laboratory, Weapons and Materials Research Directorate, ATTN: RDL-WM, Aberdeen Proving Ground, MD 21005-5069, USA*

ARTICLE INFO

Article history:
Received 25 April 2011
Accepted 14 September 2011
Available online 19 September 2011

ABSTRACT

The stacking-dependent electronic structure and transport properties of bilayer graphene nanoribbons suspended between gold electrodes are investigated using density functional theory coupled with non-equilibrium Green's functional method. We find substantially enhanced electron transmission as well as tunneling currents in the AA stacking of bilayer nanoribbons compared to either single-layer or AB stacked bilayer nanoribbons. Interlayer separation between the nanoribbons appears to have a profound impact on the conducting features of the bilayer nanoribbons, which is found to be closely related to the topology and overlap between the edge-localized π orbitals.

1. Introduction

Graphene is a two-dimensional monoatomic layer system which has attracted great research interest due to its remarkable electronic properties [1]. Its honeycomb lattice can be described in terms of an sp^2 hybridized network of carbon atoms which essentially controls the characteristic π electronic structure of graphene [2]. A pristine graphene monolayer can be cut into elongated strips to form 1D structure, referred to as graphene nanoribbons (GNRs) which can be terminated by either armchair or zigzag edges. GNRs can be either metallic or semiconducting depending on the type and width of edges [1]. Recently, the stability of edge states and edge magnetism in graphene nanoribbons is discussed, arguing that the intrinsic magnetism of GNRs may not be stable at room temperature [3].

A bilayer (b) GNR system consists of two monolayers of GNR, typically arranged in the Bernal (AB) or AA stacking arrangements. Such a bilayer system with smooth edges has been successfully fabricated by unzipping multiwalled CNTs [4], the plasma etching [5] and chemical routs [6]. It can be channel material for a field-effect transistor due to the opening of its gap by a perpendicularly applied electric field [7–9]. It has been suggested that the application of bGNRs in nanoscale electronic devices is advantageous due to their low sensitivity to external perturbations [10]. Therefore, the unique electronic properties offered by a bilayer GNR system can add another dimension to the possibility of the use of carbon-based transistors in the post-silicon era.

In a bGNR configuration, the stacking of hexagonally linked sp^2-bonded nanoribbons facilitates an interlayer interaction between π electrons which leads to the modification of its electronic properties relative to those of monolayer nanoribbons. Also, similar to the single-layer GNR, the edge chemistry is expected to have profound effect on the electronic properties of bGNR. For example, a GNR with homogeneous armchair or zigzag shaped edges is predicted to have finite gap in the ground state, with the edge states forming the top of the valence band and the bottom of the conduction band [11]. Furthermore, this gap appears to scale inversely with the width of the GNR [11]. Such an interesting electronic structure of the GNR in general and bGNR in particular has

* *Corresponding author.*
E-mail address: pandey@mtu.edu (R. Pandey).
0008-6223/$ - see front matter
doi:10.1016/j.carbon.2011.09.033

attracted a great deal of attention in their electron transport properties [5,12–16]. For the bGNR, in particular, the electron transport studies have been performed using a part of the channel-forming single-layer GNR as a contact [17,18]. Such a configuration has limited practical applications as it has the potential of introducing unwanted asymmetry in the structure. In the present study, we investigate the role of interplanar interaction in determining the transport properties of a bilayer GNR system by considering a practically realizable device configuration in which GNRs are suspended between gold electrodes. Thus, the device configuration considered in the present study is capable of exploiting the presence of the transmission channel due to the interlayer interaction between GNRs and the effect of interface between GNR and metal electrodes for electronic transport.

2. Computational model

The local spin density approximation (LDA) of the exchange [19] and correlation functional [20] forms within density functional theory, incorporated in the SIESTA program package is used [21]. It should be pointed out that the LDA-DFT method has been shown to provide reasonably good descriptions of the physics and chemistry of graphitic systems [22,23], though it underestimates the band gap of the semiconducting materials. Enhanced conductivity features in the current–voltage characteristics of the bilayer GNR configuration considered are clearly demonstrated by the LDA-DFT method employed. It is worth noting that the LDA-DFT method mimics features of the electronic band structure obtained by many-electron Green's function approach within the GW approximation reasonably well [24].

Norm-conserving pseudopotentials and double-zeta basis sets with polarization functions were used for all atoms in electronic structure calculations [21]. The k-space integration was done with a grid of $1 \times 1 \times 32$ k-points. For the contact Au atoms, the chosen Au pseudopotential and basis sets reproduce the electronic properties of the bulk Au near the Fermi region and has been successfully applied to investigate electronic transport properties of the Au–C_{60}–Au system [25].

The bias-dependent electron transmission and current are calculated using the non-equilibrium Green's functional (NEGF) method based on the Keldysh formalism, as implemented in the SMEAGOL program [26,27]. The current via the gold-connected bilayer GNRs can be obtained as

$$I = \frac{e}{h}\int_{-\infty}^{\infty} dE T(E,V)[f(E-\mu_1) - f(E-\mu_2)] \quad (1)$$

where $\mu 1$ *and* $\mu 2$ *are the electrochemical potentials in the two contacts under an external bias* V, $f(E)$ is the Fermi–Dirac distribution function. The transmission function, $T(E, V)$ is an important intrinsic factor describing the quantum mechanical transmission probabilities for electrons. The semi-infinite effect of the left (right) electrode is taken into account by introducing the self-energy ΣL (ΣR) in the effective Hamiltonian [see Supplementary information, point 1]. It is worth noting that the transmission depends on both the electron energy E and the applied external bias V.

3. Results and discussion

3.1. Structural properties

A bilayer GNR configuration consisted of hydrogen passivated zigzag graphene nanoribbons (zGNR) with a width of 13.4 Å is considered. It has six primitive cells of graphene in each unit cell and is denoted as 6-zGNR. In a zGNR, the ribbon edges order magnetically due to localization of the unpaired electrons. A parallel alignment of the spin states of both edges results into the ferromagnetic (FM) spin configuration, whereas antiparallel alignment yields the antiferromagnetic (AF) spin configuration. The calculated ground state of a pristine 6-zGNR has AF ordering between two edges, though the coupling between carbon atoms on the same edge is ferromagnetic.

The calculated results on pristine 6-zGNR employing our modeling elements agree very well with the previously reported results [11,28,29]. For example, the energy difference between AF and FM coupling of edges is about 0.006 eV per zGNR cell which is comparable with 0.004 eV per cell predicted for 8zGNR [11]. Note that Ref. [11] uses the same computation method as we do, and it is shown this energy difference decreases with zGNR width. The calculated C–C bond length varies from 1.39 Å to 1.45 Å as also predicted in earlier studies. The magnetic moment of the edge carbon atoms of bare zGNR is about 1.16 μ_B. This magnetic dipole is dramatically suppressed ($\approx$0.2 μ_B) in the presence of passivating hydrogen atoms. Since the bare (i.e. edge unpassivated) bilayer configuration of zGNRs is predicted to be unstable [30], we consider a bilayer configuration consisting of hydrogen passivated GNRs which are shown to be thermodynamically stable [11,28–31]. A full optimization of the pristine bilayer GNRs with smooth edges leads to formation of (6, 6) single-wall armchair CNT as also reported previously [30].

Following the stacking nomenclature of graphite, we classify the stacking arrangements to be either AA or AB as shown in Fig. 1; all carbon atoms of the hexagon rings are near-neighbors (i.e. top of each other) in the AA stacking whereas only half of the atoms are near neighbor and the other half of the atoms are above and below the empty centers of the hexagonal rings of GNR in the Bernal (AB) configuration. The AA bilayer only has one form of edge alignment

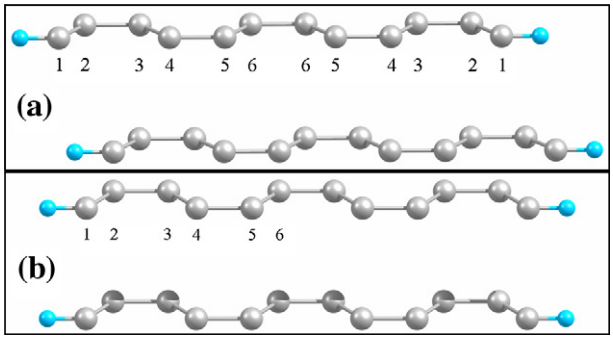

Fig. 1 – Bilayer GNR configurations (a) AB and (b) AA (C in grey and H in blue). (For interpretation of the references to color in this figure legend, the reader is referred to the web version of this article.)

whereas AB has two types of edge alignments, namely α and β alignments. Previous studies [31–33] have shown the α alignment to be energetically more stable and non-magnetic whereas the energetically less favorable β alignment does have magnetic properties [34] which can be explained by Stoner's criteria for itinerant magnetism.

The calculated results confirm the AB-α stacking arrangement to be energetically preferred for the passivated bilayer zGNRs, though the energy difference between AA and AB-α is relatively small (≈0.03 eV/atom) at the LDA-DFT level of theory. The calculated value of the binding energy of the AB-α configuration is 0.018 eV/atom in excellent agreement with the previously reported value of 0.017 eV/atom [33]. The AA stacking arrangement consisting of individually optimized 6-zGNR is predicted to be non-magnetic with an interlayer separation of 3.06 Å and binding energy of 0.015 eV/atom [see Supplementary information, point 2]. We define the binding energy to be the difference between the total energy of a bilayer and twice the value of the total energy of a passivated (AF) single-layer zGNR.

3.2. *Electronic properties*

Fig. 2 shows the electronic band structures of single-layer and bilayer 6-zGNRs along the high symmetry points in the k-space suggesting that the presence of the interlayer coupling significantly modifies the subband curvature and subband spacing of the AA stacking configuration relative to those for the AB stacked GNRs and the single-layer GNR. Note that our calculated band structures for the AB-α bilayer configuration are consistent with the results of previous theoretical study [34].

In the band structure of the passivated zGNRs, only π edge states exist due to the saturation of dangling σ edge bonds by hydrogen atoms (Fig. 2 (top)). The calculated project density of states (PDOS) of zGNR whose qualitative features agree well with the previous LDA-DFT calculations [24] is shown in Fig. 3. We find that the peaks near Fermi level can be attributed to edge atoms suggesting that the electronic bands near Fermi energy are composed of π edge states of the zGNR. The localized nature of these π edge states leads to magnetic instability in the system which opens up a gap in the band at Fermi energy. It is expected that a graphene nanoribbon with sufficiently large width is likely to mimic the band structure of a graphene sheet with zero band gap.

For the AB-α bilayer configuration, the stacking sequence facilitates the interlayer coupling which leads to a significant energy dispersion of electronic bands near Fermi surface relative to that for the single-layer GNR, though the band gap changes from 0.35 eV for single-layer GNR to 0.29 eV for the bGNR. This is in contrast to that of the AA-stacked bilayer configuration where two degenerate p_z-subbands associated with each single layer cross at the Fermi level yielding a finite density of states near Fermi energy (Fig. 3).

Fig. 3 shows the projected density of states (PDOS) on carbon atoms for single-layer and AA stacked bilayer GNR. The magnetic properties of the monolayer GNR are eliminated in the AA and AB-α GNRs leading to non-magnetic ground state of both bilayer configurations. For single-layer GNR, edge atoms dominate DOS near Fermi level (Fig. 3 (left)). The presence of the interlayer interaction between GNRs appears to shift the peaks originating from the edge states away from the Fermi level (Fig. 3 (right)); the shift is relatively larger for the AA stacking arrangement relative to that of the AB-α

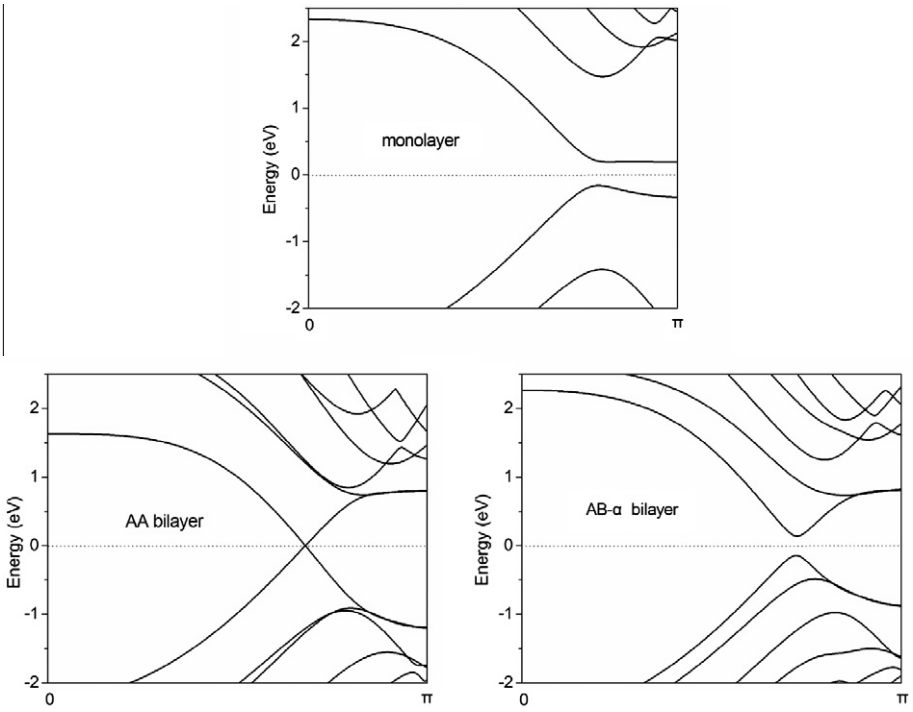

Fig. 2 – The electronic band structures of passivated zGNRs: (top) single-layer GNR, (bottom left) AA bGNR, and (right) AB-α bGNR. Zero of the energy is aligned to the Fermi energy.

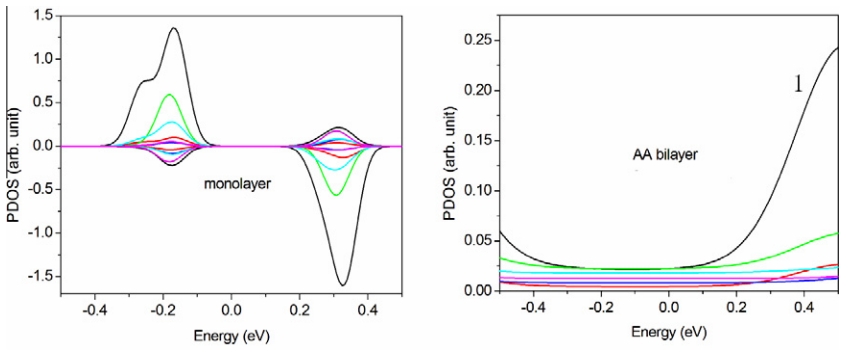

Fig. 3 – Density of states (DOS) projected on carbon atoms of passivated zGNRs: (left) single-layer GNR, (right) AA bGNR. Black, red, green, blue, cyan and magenta represent the PDOS associated with the 1st, 2nd, . . . , 6th carbon atom counted from ribbon edge to the central region, as shown in Fig. 1. For the case of single-layer GNR, both spin up and spin-down components of PDOS are shown. Zero of the energy is aligned to the Fermi energy. (For interpretation of the references to color in this figure legend, the reader is referred to the web version of this article.)

stacking arrangements. This effect is more pronounced in the AA stacking of GNRs because of significant interlayer bonding between all carbon atoms on top and bottom GNRs. In contrast, only half of the carbon atoms in the AB stacking of the bGNR interact significantly. Thus, as expected, the AB-α stacking has an interlayer coupling strength between the AA stacking and the single-layer GNR. Consequentially, the single-layer GNR has a finite gap and is magnetic, the AB-α stacked bilayer has a finite gap and is non-magnetic, and the AA stacked bilayer GNR is non-magnetic with zero gap.

The topology of the AA stacked bilayer GNR appears to be the dominant factor in predicting its zero gap. Note that the existence of the energy gap in single-layer zGNR is associated with the (unsaturated) dangling bonds associated with edge atoms. On the other hand, the interaction between edge atoms is facilitated by the topology of the AA stacked bilayer leading to crossing of the bands at Fermi level. This is confirmed in Fig. 4 where we have examined the evolution of band structure of the AA GNR with the change in its interlayer spacing. For a large interlayer spacing of 5.94 Å, each band is twofold degenerate due to negligible interaction between the two passivated single-layer GNRs. The calculated band gap is the same as that of the single-layer GNR. As the interlayer separation between the GNRs decreases, the

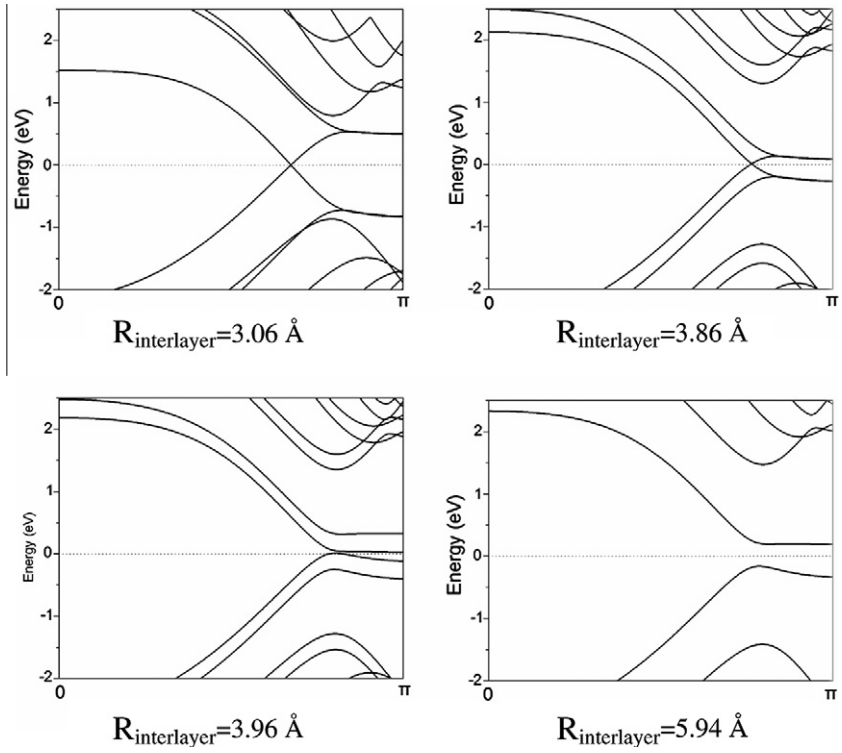

Fig. 4 – The electronic band structures of the AA bGNRs as a function of the interlayer spacing. Zero of the energy is aligned to the Fermi energy.

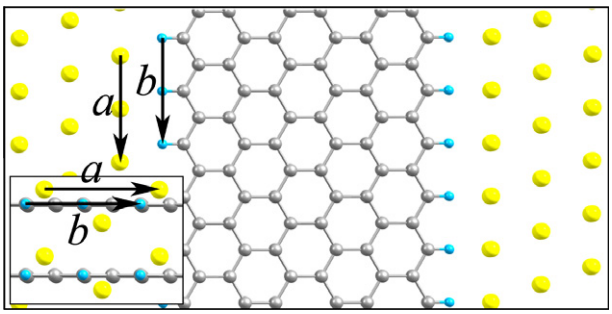

Fig. 5 – A top view of the suspended passivated AA bGNR coupled with semi-infinite bulk gold electrodes. The insert shows the lattice matching of GNR and gold leads. Symbols: C in grey, H in blue, and Au in yellow. (For interpretation of the references to color in this figure legend, the reader is referred to the web version of this article.)

coupling between the two begins to dominate in determining the band structure; eventually leading to the crossing of linear valence and conduction bands at the Fermi level (Fig. 4).

3.3. *Transport properties*

The Au (111) surface is chosen to be the contact lead for transport calculations since its lattice parameter matches well with that of the GNR, thus minimizing the interfacial lattice distortions in the device configuration. The lattice vector '**a**' of Au (111) has a length of 5.00 Å, while the double length of GNR shown as vector '**b**' is 4.92 Å, as shown in Fig. 5. The contact distance is taken to be 2 Å yielding the distance between left and right gold electrodes to be 17.4 Å. There exists a weak interaction between the gold contact and the passivated GNR.

Consequently, Au atoms do not lead to charge transfer or doping in GNRs as also reported previously [35]. Note that the passivated GNR is infinitely long with a width of 13.4 Å, as a 1D structure, and the electron transport direction is along the width.

The *I–V* characteristics of the AA bilayer and monolayer configurations are shown in Fig. 6. The results predict substantial device conduction for AA relative to that of monolayer. This is consistent with the calculated band structure

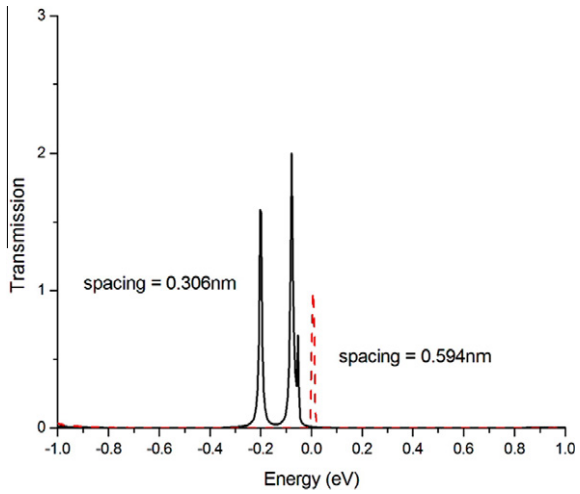

Fig. 7 – The transmission function of the AA bGNR at zero bias: (i) (dotted line) interlayer spacing = 0.594 nm and (ii) (solid line) interlayer spacing = 0.306 nm. Zero of the energy is aligned to the Fermi energy.

and density of states of these configurations. The calculated current of the AA bilayer equilibrium configuration at a given bias cannot be regarded as a sum of current due to individual GNRs. At a relatively large interlayer spacing (~6 Å), the calculated current is indeed approximately twice the current calculated for a monolayer passivated GNR (Fig. 6). We notice that the increase in the interlayer spacing does not change the details of gold contacts with the GNRs, keeping the interfacial configurations to be the same. We have also calculated the electronic transport properties of the AB bilayer configuration predicting a much smaller current compared with the AA-stacked bilayer at a given bias [see, Supplementary information, Figure S1]. Considering the asymmetric coupling to electrodes on the left and right side of each layer of GNR for the AB bilayer, a larger vacuum gap acts as a higher energy barrier decreasing the current at a given bias.

Analysis of transmission functions shown in Fig. 7 confirms the role of interlayer coupling in facilitating the transmission channel for the AA stacking arrangement for the passivated zGNRs. An additional inter-band state appears in the vicinity of the Fermi level with a decrease in the interlayer

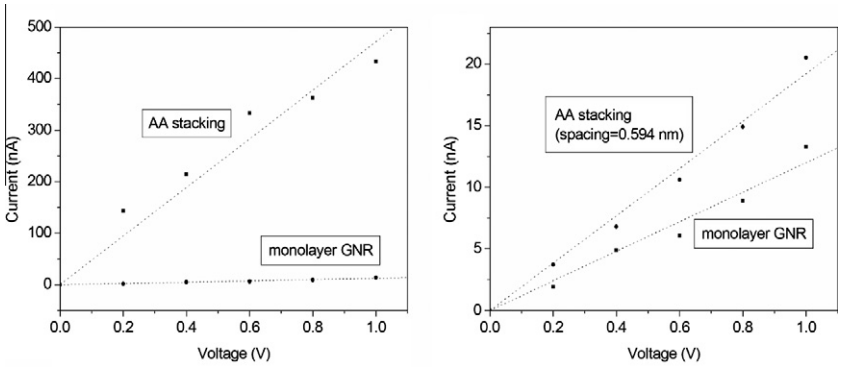

Fig. 6 – *I–V* characteristics of the single-layer GNR and the AA bGNR (left) AA bGNR with the equilibrium interlayer spacing of 0.306 nm, (right) AA bGNR with a large interlayer spacing of 0.594 nm.

separation of the bilayer GNRs. Thus, the interlayer interactions mainly due to delocalized π electronic states in the AA stacked bilayer appear to play a critical role on the metal-like conducting behavior of these GNRs.

We note that our results are not in agreement with the results of (spin-unpolarized) tight binding method calculations [36] in which the AB stacked bilayer GNR was reported to be semi metallic with the finite density of states at Fermi level. Recent first principles investigations considering spin-polarization terms [11,32,33] showed that both monolayer zGNR and AB stacked bilayer zGNR have a finite gap at Fermi level as also predicted in our study.

4. Summary

First principles electronic structure calculations together with non-equilibrium Green's Function method were performed on a bilayer GNR system in two different stacking arrangements. The calculations reveal that a bilayer GNR system in the AA stacking configuration exhibits substantially enhanced electron transmission as well as tunneling currents compared to single-layer GNRs. The AA bGNR system has a non-vanishing transmission near Fermi energy. In contrast, either a single-layer or AB-α bilayer GNRs has a large transmission gap. The calculated enhanced conducting features of the AA bilayer are closely related to the interacting π-orbitals of the two GNRs. Considering that the graphene bilayers with the AA stacking configuration can be synthesized [37], their predicted enhanced conductivity suggest them to play a an important role in the development of future nanoscale electronic devices.

Acknowledgments

Helpful discussions with Dr. Ranjit Pati and Saikat Mukhopadhyay are acknowledged. The work at Michigan Technological University was performed under support by the Army Research Office through Contract Number W911NF-09-1-0221.

Appendix A. Supplementary data

Supplementary data associated with this article can be found, in the online version, at doi:10.1016/j.carbon.2011.09.033.

REFERENCES

[1] Abergel DSL, Apalkov V, Berashevich J, Ziegler K, Chakraborty T. Properties of graphene: a theoretical perspective. Adv Phys 2010;59(4):261.
[2] Nakada K, Fujita M, Dresselhaus G, Dresselhaus MS. Edge state in graphene ribbons: nanometer size effect and edge shape dependence. Phys Rev B 1996;54(24):17954.
[3] Kunstmann J, Ouml zdogbrevean C, Quandt A, Fehske H. Stability of edge states and edge magnetism in graphene nanoribbons. Phys Rev B 2011;83(4):045414.
[4] Jiao L, Zhang L, Wang X, Diankov G, Dai H. Narrow graphene nanoribbons from carbon nanotubes. Nature 2009;458(7240):877.
[5] Han MY, Ouml zyilmaz B, Zhang Y, Kim P. Energy band-gap engineering of graphene nanoribbons. Phys Rev Lett 2007;98(20):206805.
[6] Li XL, Wang XR, Zhang L, Lee SW, Dai HJ. Chemically derived, ultrasmooth graphene nanoribbon semiconductors. Science 2008;319(5867):1229.
[7] Oostinga JB, Heersche HB, Liu X, Morpurgo AF, Vandersypen LMK. Gate-induced insulating state in bilayer graphene devices. Nat Mater 2008;7(2):151.
[8] Szafranek BN, Schall D, Otto M, Neumaier D, Kurz H. Electrical observation of a tunable band gap in bilayer graphene nanoribbons at room temperature. Appl Phys Lett 2010;96(11):112103.
[9] Sai-Kong C, Dawei S, Kai-Tak L, Samudra GS, Gengchiau L. Device physics and characteristics of graphene nanoribbon tunneling FETs. Electron Dev IEEE Trans 2010;57(11):3144.
[10] Lin YM, Avouris P. Strong suppression of electrical noise in bilayer graphene nanodevices. Nano Lett 2008;8(8):2119.
[11] Son YW, Cohen ML, Louie SG. Energy gaps in graphene nanoribbons. Phys Rev Lett 2006;97(21):216803.
[12] Barraza-Lopez S, Vanević M, Kindermann M, Chou MY. Effects of metallic contacts on electron transport through graphene. Phys Rev Lett 2010;104(7):076807.
[13] Wang X, Ouyang Y, Li X, Wang H, Guo J, Dai H. Room-temperature all-semiconducting sub-10-nm graphene nanoribbon field-effect transistors. Phys Rev Lett 2008;100(20):206803.
[14] Wakabayashi K, Takane Y, Yamamoto M, Sigrist M. Electronic transport properties of graphene nanoribbons. New J Phys 2009;11:055054.
[15] Chen JC, Cheng SG, Shen SQ, Sun QF. Electronic transport through a graphene-based ferromagnetic/normal/ferromagnetic junction. J Phys Condens Matter 2010;22(3):035301.
[16] Chang SL, Tsai CH, Su WS, Chen SC, Lin MF. Electronic properties of bilayer AA-stacked zigzag nanographene ribbons. Diam Relat Mater 2011;20(4):505.
[17] Li TS, Huang YC, Chang SC, Chuang YC, Lin MF. Transport properties of AB-stacked bilayer graphene nanoribbons in an electric field. Eur Phys J B 2008;64(1):73.
[18] Bhattacharya S, Mahapatra S. Negative differential conductance and effective electron mass in highly asymmetric ballistic bilayer graphene nanoribbon. Phys Lett A 2010;374(28):2850.
[19] Ceperley DM, Alder BJ. Ground state of the electron gas by a stochastic method. Phys Rev Lett 1980;45(7):566.
[20] Perdew JP, Zunger A. Self-interaction correction to density-functional approximations for many-electron systems. Phys Rev B 1981;23(10):5048.
[21] José MS, Emilio A, Julian DG, Alberto G, Javier J, Pablo O, et al. The SIESTA method for ab initio order-N materials simulation. J Phys: Condens Matter 2002;14(11):2745.
[22] Trickey SB, Müller-Plathe F, Diercksen GHF. Interplanar binding and lattice relaxation in a graphite dilayer. Phys Rev B 1992;45(8):4460.
[23] Marini A, García-González P, Rubio A. First-principles description of correlation effects in layered materials. Phys Rev Lett 2006;96(13):136404.
[24] Yang L, Park C-H, Son Y-W, Cohen ML, Louie SG. quasiparticle energies and band gaps in graphene nanoribbons. Phys Rev Lett 2007;99(18):186801.
[25] Zhong X, Pandey R, Rocha AR, Karna SP. Can single-atom change affect electron transport properties of molecular nanostructures such as C60 fullerene? J Phys Chem Lett 2010;1(10):1584.
[26] Rocha AR, García-Suárez VM, Bailey S, Lambert C, Ferrer J, Sanvito S. Spin and molecular electronics in atomically generated orbital landscapes. Phys Rev B 2006;73(8):085414.

[27] Rocha AR, Garcia-suarez VM, Bailey SW, Lambert CJ, Ferrer J, Sanvito S. Towards molecular spintronics. Nat Mater 2005;4(4):335.
[28] Lee H, Son Y-W, Park N, Han S, Yu J. Magnetic ordering at the edges of graphitic fragments: magnetic tail interactions between the edge-localized states. Phys Rev B 2005;72(17):174431.
[29] Wassmann T, Seitsonen AP, Saitta AM, Lazzeri M, Mauri F. Structure, stability, edge states, and aromaticity of graphene ribbons. Phys Rev Lett 2008;101(9):096402.
[30] Saxena S, Tyson TA. Ab initio density functional studies of the restructuring of graphene nanoribbons to form tailored single walled carbon nanotubes. Carbon 2010;48(4): 1153.
[31] Barone V, Hod O, Scuseria GE. Electronic structure and stability of semiconducting graphene nanoribbons. Nano Lett 2006;6(12):2748.
[32] Sahu B, Min H, MacDonald AH, Banerjee SK. Energy gaps, magnetism, and electric-field effects in bilayer graphene nanoribbons. Phys Rev B 2008;78(4):045404.
[33] Lima MP, Fazzio A, da Silva AJR. Edge effects in bilayer graphene nanoribbons: Ab initio total-energy density functional theory calculations. Phys Rev B 2009;79(15):153401.
[34] Guo Y, Guo W, Chen C. Semiconducting to half-metallic to metallic transition on spin-resolved zigzag bilayer graphene nanoribbons. J Phys Chem C 2010;114(30):13098.
[35] Pinto H, Jones R, Goss JP, Briddon PR. Unexpected change in the electronic properties of the Au-graphene interface caused by toluene. Phys Rev B 2010;82(12):125407.
[36] Sun SJ, Chang CP. Ballistic transport in bilayer nano-graphite ribbons under gate and magnetic fields. Eur Phys J B – Condens Matter Complex Syst 2008;64(2):249.
[37] Liu Z, Suenaga K, Harris PJF, Iijima S. Open and closed edges of graphene layers. Phys Rev Lett 2009;102(1):015501.